Biogeosciences Discuss., 8, 7953–8000, 2011
www.biogeosciences-discuss.net/8/7953/2011/
doi:10.5194/bgd-8-7953-2011

Biogeosciences Discussions

Redox sensitive elements in foraminifera from the Peruvian oxygen minimum zone

N. Glock[1,2], A. Eisenhauer[2], V. Liebetrau[2], M. Wiedenbeck[3], C. Hensen[2], and G. Nehrke[4]

[1]Sonderforschungsbereich 754, Christian-Albrechts-University Kiel, Climate-Biogeochemistry Interactions in the Tropical Ocean, Germany
[2]Leibniz-Institute für Meereswissenschaften, IFM-GEOMAR, Wischhofstr. 1–3, 24148 Kiel, Germany
[3]Helmholtz-Zentrum Potsdam, GFZ German Research Centre for Geosciences, Telegrafenberg, 14473 Potsdam, Germany
[4]Alfred Wegener Institut für Polar- und Meeresforschung, Am Handelshafen 12, 27570 Bremerhaven, Germany

Received: 3 August 2011 – Accepted: 4 August 2011 – Published: 8 August 2011

Correspondence to: N. Glock (nglock@ifm-geomar.de)

Published by Copernicus Publications on behalf of the European Geosciences Union.

Abstract

Testing order to assess their potential as a proxy for redox conditions the element/Ca ratios of the redox sensitive elements Mn and Fe were determined in tests of benthic foraminifera from the Peruvian oxygen minimum zone (OMZ). Prior to the determination of the element/Ca ratios the distributions of Ca, Mn, Fe, Mg, Ba, Al, Si, P and S in tests of the shallow infaunal species *Uvigerina peregrina* and *Bolivina spissa* were mapped with an electron microprobe (EMP). An Fe rich phase which is also enriched in Al, Si, P and S was found on the inner test surface of *U. peregrina*. The element distributions of a specimen treated with an oxidative cleaning procedure show the absence of this phase. EMP maps of *B. spissa* also identified a similar phase which too could be removed with oxidative cleaning. Neither in *B. spissa* nor in *U. peregrina* were any hints for diagenetic (oxyhydr)oxide or carbonate coatings found. Mn/Ca and Fe/Ca ratios of single specimens of *B. spissa* from different locations have been determined by secondary ion mass spectrometry (SIMS). Bulk analyses using solution ICP-MS of several samples were compared to the SIMS data. The difference between SIMS analyses on single specimens and ICP-MS bulk analyses from the same sampling sites was 14.0–134.8 µmol mol^{-1} for the Fe/Ca and 1.68 µmol mol^{-1} for the Mn/Ca ratios. This amounts to 3–29 % for the Fe/Ca and 21.5 % for the Mn/Ca ratios of the overall variability between the samples of the different sampling sites. The Mn/Ca ratios in the calcite were generally relatively low (2.21–9.93 µmol mol^{-1}) but of the same magnitude as in the pore waters (1.37–6.67 µmol mol^{-1}). Comparison with sediment pore water data showed that Mn/Ca in the foraminiferal calcite is proportional to the Mn/Ca ratio in the top cm of the pore water. The lowest Fe/Ca ratio in tests of *B. spissa* (87.0 µmol mol^{-1}) has been found at a sampling site which was strongly depleted in oxygen and showed a high, sharp iron peak in the top interval of the pore water. This, and the fact that at this location many dead but no living specimens were found during sampling time, hints that the specimens already were dead before the Fe flux started and the sampling site just recently turned anoxic due to fluctuations of the lower boundary of the OMZ where the sampling site is located (465 m water depth).

BGD

8, 7953–8000, 2011

1 Introduction

Various element to Ca ratios in foraminiferal calcite have been widely used to reconstruct chemical or physical properties in the ancient ocean. Well established is the temperature reconstruction using the Mg/Ca ratio (Nürnberg et al., 1996; Rosenthal et al., 1997; Hastings et al., 1998; Lea et al., 1999; Elderfield and Ganssen, 2000; Lear et al., 2002). But other proxies are utilized, too like the U/Ca ratio for redox state, seawater chemistry and CO_3^{2-} tracing (Russel et al., 1994, 2004; Yu et al., 2008), Zn/Ca ratios for carbonate saturation (Marchitto et al., 2000) and Cd/Ca ratios as phosphate tracer (Boyle and Keigwin, 1985; Boyle, 1988; Bertram et al., 1995, Came et al., 2003). Recently a lot attention turned to the analyses of boron isotopes in foraminiferal calcite for pH reconstruction via $\delta^{11}B$ (Spivack et al., 1993; Sanyal et al., 1995; Palmer et al., 1998; Pearson and Palmer, 2000; Sanyal et al., 2001; Palmer and Pearson, 2003; Ni et al., 2007; Foster, 2008; Kasemann et al., 2009; Rollion-Bard and Erez, 2010; Rae et al., 2011). The V/Ca ratio has been suggested as a proxy for redox-conditions (Hastings et al., 1996a, b, c) while the Ba/Ca ratio has been shown to occur in direct proportion to seawater concentration (Lea and Boyle, 1991; Lea and Spero, 1992, 1994). Ba/Ca ratios have already been used to trace deglacial meltwater (Hall and Chan, 2004a) and deep and intermediate water mass circulation (Lea and Boyle, 1989, 1990a, b; Martin and Lea, 1998; Hall and Chan; 2004b).

Fossil foraminifera often show diagenetic coatings which strongly influence the measured element/Ca ratios and thus rigorous cleaning techniques have to be deployed. About three decades ago a procedure to remove these contaminants by rinsing crushed tests with distilled water/methanol to remove adhesive clays followed by a reductive cleaning step to remove metal oxide coatings has been developed (Boyle, 1981). Later a procedure was developed to get rid of organic contaminations by using an additional oxidative cleaning step (Boyle and Keigwin, 1985). The influence of the different cleaning steps on the Mg/Ca ratios has been tested and it has been shown that the clay removal step is the most important one while the reductive cleaning step

BGD
8, 7953–8000, 2011

produces a down offset of about 10–15 % on the Mg/Ca ratios (Barker et al., 2003). Different cleaning techniques and their influence on eight elemental/Ca ratios have also been investigated by Yu et al. (2007). Also there have been experiments of cleaning by using a flow-through system with automated chromatographic equipment (Haley and Klinkhammer, 2002; Haley et al., 2005). In the system contaminant phases are chemically removed from the tests and the cleaned calcite is then dissolved in a stream of weak acid. The advantage of this method is that the different fractions could be collected separately and the measurements of contamination tracers like Fe could show in which fractions only clean dissolved foraminiferal calcite is collected. Furthermore the flow-through system could minimize the problem of re-adsorption of contaminant rare-earth-elements. As diagenetic contaminant phases Mn carbonates have been identified as well as Mn and Fe rich oxyhydroxides with laser-ablation-ICP-MS (LA-ICP-MS) and electron microprobe (EMP) mapping (Pena et al., 2005, 2008). Mn/Ca and Fe/Ca ratios therefore have often been used as tracer for diagenetic overprint of the samples. Nevertheless the researcher disagree what is considered an acceptable level of test Mn/Ca from 50 µmol mol^{-1} to >150 µmol mol^{-1} (Boyle, 1983; Boyle and Keigwin, 1985, 1986; Delaney, 1990; Ohkouchi et al., 1994, Lea, 2003). But there exist approaches to use Mn/Ca ratios during the obvious absence of diagenetic coatings as a proxy for redox-conditions, too. The Mn/Ca ratio in *Hoeglundina elegans* has been used to trace suboxic conditions during sapropel formation (Fhlaitheartha et al., 2010). Also living stained specimens of *H. Elegans* from the oxygen minimum zone at the Arabian Sea show an increase of the Mn/Ca ratio at the lower boundary of the oxygen minimum zone (Reichart et al., 2003). Culture experiments on *Ammonia tepida* showed that Mn is incorporated into the test calcite in proportion to the concentration in the ambient water (Munsel et al., 2010).

Several analytical techniques have been employed for analyses of element/Ca ratios or isotope systems in foraminiferal calcite. Techniques for multi-element analyses using only small sample volumes have been developed on sector field ICP-MS (Marchitto, 2006) and quadrupole ICP-MS (Yu et al., 2005; Harding et al., 2006). But also

BGD
8, 7953–8000, 2011

microanalytic methods, which allow analysing single specimens locally, have been deployed. The advantage of the EMP is that single foraminiferal tests can be analysed with comparable low damage at the surface after preparation of polished sections. These sections can be remeasured after renewed grinding and polishing. This is an important prerequisite for comparison with other low trace methods like secondary ion mass spectrometry (SIMS). Both elemental mapping by means of EMP and spot analyses of test calcite can help identify contaminant coatings and can characterise the distributions of trace elements inside the foraminiferal calcite, improving the usability of element to Ca ratios as paleoenvironmental proxies (Nürnberg, 1995; Nürnberg et al., 1996; Eggins et al., 2003, 2004; Sadekov, 2005; Toyofoko and Kitazato, 2005; Pena et al., 2008). Also laser ablation techniques on single foraminifera have been used in the recent past (Wu and Hillaire-Marcel, 1995; Hathorne et al., 2003; Reichart et al., 2003; Pena, 2005; Munsel et al., 2010).

A second valuable tool for foraminiferal microanalyses is SIMS. With good sample preservation after analysis in the same way as the EMP, SIMS has been used to produce element mappings and determine element/Ca ratios in foraminiferal calcite (Allison and Austin, 2003; Sano et al., 2005; Bice et al., 2005; Kunioka et al., 2006) as well as analyses of δ^{11}B in single foraminifera (Kasemann et al., 2008; Rollion-Bard and Erez, 2009) and the determination of intratest variability of δ^{18}O (Rollion-Bard et al., 2008). Other powerful, though less widely available techniques like particle induced x-ray emission (Gehlen et al., 2004) or μ-synchroton XRF (Munsel et al., 2010) have also been empolyed in foraminifera studies. All these microanalytical techniques have in common that analyses could be deployed even on single foraminiferal specimens whereas wet chemical analyses typically require 20–50 specimens of smaller foraminiferal species; obviously microanalytical methods are favourable when there is only a very limited number of specimens available or when an assessment of chemical heterogeneity is required.

In this study the shallow infaunal species *Bolivina spissa* is used for the determination of Fe/Ca and Mn/Ca ratios, measured with SIMS and ICP-MS, and the comparison

BGD
8, 7953–8000, 2011

of these ratios to the available pore water data. Because of the relative widespread distribution among the Peruvian OMZ *B. spissa* was available from habitats with a wide range of redox-chemical conditions although at some sampling sites only a small amount of specimens was available. SIMS was used because only a low number of specimens was available in several samples. If enough specimens for bulk analysis where available in a sample SIMS was compared to ICP-MS data. Studies on the pore density in *B. spissa* showed a morphological adaptation of the test to different environmental conditions (Glock et al., 2011) which makes this species favourable for elemental analyses, too.

2 Material and methods

2.1 Sampling procedure

Six short (12–26 cm) sediment cores from the Peruvian OMZ were considered for the present study (Table 1). The cores were recovered by using multicore technology during R/V *Meteor* cruise M77/1 in October and November 2008. Within a couple of minutes after the multicorer came on deck, one tube was chosen from the array, and brought to a laboratory having a constant room temperature of 4 °C. Supernatant water of the core was carefully removed. Then the core was gently pushed out of the multicorer tube and cut into 10-mm-thick slices for benthic foraminiferal analysis. The samples were transferred to Whirl-Pak™ plastic bags and transported at a temperature of 4 °C. One core was completely frozen, and later sliced and sub-sampled at IFM-GEOMAR, Kiel. The samples from these five cores were used to collect the foraminiferal specimens for the analysis.

BGD
8, 7953–8000, 2011

2.2 Foraminiferal studies

The surface sediment samples corresponding to the top centimeter were washed over a 63 µm mesh sieve. The residues were collected in ethanol to prevent samples from dissolution and dried at 50 °C. They were further subdivided into the grain-size fractions of 63–125, 125–250, 250–315, 315–355, 355–400, and >400 µm. Specimens of the shallow infaunal species *B. spissa* for ICP-MS and SIMS analysis were picked from the 125–250 µm fraction, specimens of *Uvigerina peregrina* for the microprobe analyses were picked from the 355–400 µm fraction.

2.3 Cleaning methods

For each ICP-MS analysis a bulk sample of 40 specimens of *B. spissa* was used. The tests were gently crushed between two glass plates. The test fragments were transferred into PE vials and rinsed three times with reverse osmosis water (ROW) having a conductivity of 0.055 µS cm^{-1} (Elga™ PURELAB Ultra). After each rinsing step the vials were put into a ultrasonic bath for 20 s. Afterwards the vials were rinsed three times with methanol and put into the supersonic bath for 1 min after each rinsing step. The vials were rinsed again two times with ROW to remove residual methanol. An oxidative reagent was freshly mixed by adding 100 µl 30 % H_2O_2 to 10 ml of a 0.1M NaOH (p.a., Roth™) solution. Subsequently 350 µl of this reagent were added to each vial. The vials were put into a waterbath at 92 °C for 20 min. After another 20 s in the supersonic bath the vials were rinsed two times with ROW to remove residues of the oxidative reagent. The test fragments were transferred into clean vials with a pipette. Into each vial 250 µl 0.001M HNO_3 (suprapure, Roth™) were added. The vials were put into the ultrasonic bath for 20 s. The extremely low acidic solution was removed and the vials were rinsed three times with ROW. The samples were dissolved in 300 µl 0.075M HNO_3 (suprapure, Roth™), centrifuged and transferred into clean vials. Due to the risk of elevated Mn blanks the vials were replaced by Teflon beakers for Mn

BGD
8, 7953–8000, 2011

analyses (except for the cleaning step with 0.001M HNO_3 (suprapure, Merck™), the sample dissolution and the centrifugation). The cleaning procedure for the microanalyses was in general the same with a few exceptions. The specimens were not crushed and one vial was used for one single specimen. The first three rinsing steps with ROW were skipped because specimens often lifted to the surface and got lost during the rinsing steps. The specimens were not transferred into a clean vial after the oxidative cleaning step and were not dissolved. After the last cleaning step the specimens were individual collected over a 125 µm mesh stainless steel sieve.

2.4 Microdrilling of the Oka calcite grain

A matrix matched reference material was required in order to quantify SIMS trace element analyses. Using a New Wave Research™ micromill a square having a 400 µm and 200 µm thickness was extracted from a calcite crystal from the OKA carbonatite complex for which Mg/Ca and Sr/Ca ratios have been reported by Gaetani and Cohen (2006). The resulting powder was collected in a Teflon beaker and dissolved in 2 % HNO_3. A polished piece from the same OKA calcite crystal was subsequently used in this study as reference material for SIMS after Mn/Ca and Fe/Ca ratios were determined by solution ICP-MS on the micromilled powder.

2.5 Preparation of crosssections for SIMS and microprobe analyses

The crosssection of the *U. peregrina* specimen shown in Fig. 1 was prepared at the Alfred-Wegener-Institute Bremerhaven. The specimen was embedded in Araldite™ epoxy resin under vacuum inside a stainless steel chamber. Afterwards the chamber was set under pressure to eliminate any voids inside the resin after which the resin was hardened at 60 °C. The resin was ground down with alumo-silica grinding paper until the centre of the specimen was exposed. Subsequently the surface was polished using a silk cloth and 3 µm diamond suspension followed by a final polishing step using 0.3 µm

BGD
8, 7953–8000, 2011

Al_2O_3 suspension. After each polishing step the surface was cleaned in a supersonic bath for a few seconds.

All other cross-sections were prepared at the IFM-Geomar in Kiel. The *U. peregrina* specimens shown in Figs. 2 and 3 were embedded in epoxy resin under laboratory atmosphere. Afterwards they were ground by hand using alumu-silica grinding paper until the chambers were opened. Because the chambers were not filled with resin small drops of resin were used to fill the inner part of the chambers. The surface was then polished by hand with 5 µm diamond paste followed by 1 µm alumo-silica paste using a rotating polishing plate. After each polishing step the surface of the sample mount was cleaned in an ultrasonic bath for several seconds. All other specimens including all specimens of *B. spissa* were embedded under vacuum into Araldite™ epoxy resin using the CitoVac™ vacuum embedding system by Struehrs™. The resin was ground down with alumo-silica grinding paper with the Tegra-Pol-21 system by Struehrs™ until the centre of the specimen was fully exposed. Afterwards the surface was polished with different grain sizes of alumo-silica and diamond paste until 1 µm grain size. After each polishing step the surface was cleaned in an ultrasonic bath for several seconds.

2.6 Electron microprobe mapping

A JEOL JXA 8200 electron microprobe was used to generate element distribution maps for Ca, Mn, Fe, Mg, Ba, Al, Si, S and P within cross-sections of benthic foriminiferal test walls. Each cross-section was carbon coated before the measurements. The microprobe was operated in a wavelength dispersive mode by using different Kα X-ray lines for each element. Up to five spectrometers could be used to measure up to five elements simultaneously. The different spectrometer crystals which were used for the different elements are listed in Table 2. An acceleration voltage of 15 kV and a beam current of 20 nA was used. The selected areas were mapped by using a step size of 0.5 µm and a dwell time of 500 ms. Results are illustrated as maps of relative measured

BGD
8, 7953–8000, 2011

intensities for the different elements. The JEOL JXA 8200 was also used to generate the secondary electron images of the foraminiferal cross-sections.

2.7 SIMS analyses

The Mn/Ca and Fe/Ca ratio analyses in test cross-sections of *B. spissa* were performed using a Cameca ims 6f magnetic sector ion microprobe at the Helmholtz Centre Potsdam. Each cross-section was ultrasonically cleaned twice in high purity ethanol prior to coating with a 35 nm thick, high purity gold coat.

Analyses used a 200 pA, nominally 12.5 kV, mass filtered $^{16}O^-$ ion-beam which was focused to a diameter of circa 4 µm on the sample surface (Fig. 9). Prior to each analysis the analytical location was presputtered for 300 s with the beam rastered over 10 × 10 µm raster followed by a second 3 min preburn with a static beam. During the first presputtering the $^{40}Ca^+$ distribution was monitored using the dynamic ion imaging system of the instrument in order to improve the beam targeting on the thin walls of the test being investigated.

The mass spectrometer of the SIMS was operated at a mass resolution $M/\Delta M \approx 6000$, which is required in order to separate the ^{55}Mn peak from the isobaric $^{54}Fe^1H$ molecule. A 150 µm contrast aperture was used in conjunction with a 750 µm field aperture (equivalent to a 60 µm diameter field of view); no energy offset was employed and a 50 V wide energy window was used. A single analyses consisted of 30 scans of the sequence 39.95 Da (0.1 s per cycle, used during the spot preburn), ^{40}Ca (2 s), ^{55}Mn (10 s), ^{56}Fe (4 s) and ^{63}Cu (4 s), resulting in a total data acquisition time of roughly 10 min.

The OKA calcite was used as a reference material to convert the observed Mn/Ca and Fe/Ca count rate ratios into µmol mol^{-1} concentration values. It was analysed a total of $n = 14$ times during our July 2010 analytical session, yielding a 1 sd repeatability of 1.5 % for the observed Mn/Ca, 14.8 % for Fe/Ca and 23.2 % for Cu/Ca ratios.

The test walls of *B. spissa* are generally quite thin (about 10–20 µm thickness). The test is perforated; however the pores with a diameter of about 6 µm are relatively big

BGD
8, 7953–8000, 2011

and easy to see on secondary electron images of the cross-sections. Each analysis targeted a region of a test wall that had few or no pores so as to minimize any potentially contamination accumulated inside the pores. Subsequent to our SIMS session secondary electron images were made of the cross-sections in order to assess whether that SIMS ion beam was well focused and centered on the middle of the test wall. Measurements which were obviously done partly on epoxy or at the edge of the test wall or which showed low Ca count rates were discarded. All Cu measurements showed unexpectedly high ^{63}Cu, for which we do not have an explanation. The Cu measurements have not been used in the data evaluation.

2.8 Quadrupole ICP-MS analyses

The analyses were performed on an Agilent 7500cx quadrupole ICP-MS. Operation conditions are listed in Table 3. Instrument sensitivity was optimised by using of a 1 ppb Li-Y-Tl-Ce-Mg-Co standard solution before the measurements. For sample introduction a micro-autosampler (Cetac ASX 100) coupled to a PFA self-aspiration nebulizer fitted to a glass spray chamber was used. Due to the small available sample volume (typically >500 µl) the low sample uptake rate of the self aspiration system was an important feature during the analyses. The integration times were 0.1 s for ^{48}Ca, 1 s for ^{55}Mn and 2 s for ^{56}Fe with 3 repetition runs. An octopole collision cell flooded with H_2 as reaction gas was used during the ^{56}Fe analyses to minimize interferences with ^{40}Ar^{16}O.

Dillutions were prepared from certified ICP-MS grade stock solutions (10 000 ppm for Ca, 1000 ppm for Fe and Mn) by dilution with 2 % HNO_3. The working standards were made by mixing the dilutions with 2 % HNO_3 to give Ca concentrations of 10 ppm and Fe/Ca and Mn/Ca ratios in the magnitude of foraminiferal calcite. The concentrations for the different standard rows are listed in Table 4. A second standard row with higher Mn concentrations was prepared for the analyses of the Mn/Ca ratio in the OKA as well as a standard row for determination of Ca concentrations. About 50 µl of the samples were diluted to 250 µl first for the analyses of the Ca content. The remainder was diluted to 10 ppm Ca to overcome matrix effects during the element ratio determinations.

BGD
8, 7953–8000, 2011

2.9 Pore water data

All pore-water data, discussed in this work are taken from Scholz et al. (2011).

3 Results

3.1 EMP mappings of *U. peregrina* tests

Several trace element distribution maps on uncleaned tests of *U. peregrina* and the associated SEM pictures are shown in Figs. 1–3. Strong Mg-bends which are typical for the primary calcite in tests of bilaminated calcitic foraminifera can be seen nicely in Fig. 1. The inner parts of the wall are highly enriched in iron. A slight iron enrichment is also present in the pores. The iron rich phase at the inner surfaces of the wall furthermore is enriched in Al, Si, P and S (Figs. 2 and 3) which hints towards a presence of alumo-silicates (clays) and organic matter. There are muddy accumulations present inside the chambers. These accumulations differ in their chemical composition from the iron rich phase at the inner parts of the wall (less Fe and Ca, more S and P) (Fig. 2). The chemical composition of two cuts directly through layers of this iron rich phase is shown in Fig. 3. The element mapping shows nicely the transition from the calcitic test walls into this iron rich phase. A trace element distribution map in a test section of an *U. peregrina* specimen treated with an oxidative cleaning is shown in Fig. 4. In contrast to the element maps of the uncleaned specimens this specimen does not show an iron rich phase attached to the inner surface of the test.

3.2 EMP mappings of *B. spissa* tests

Several trace element distribution maps on tests of *B. spissa* are shown in Figs. 5–7. Maps are shown for uncleaned (Fig. 5) and cleaned specimens (Figs. 6 and 7). In contrast to *U. peregrina B. spissa* does not show Mg-bands in the test walls. The inner parts of the test wall of the uncleaned specimen (Fig. 5) are enriched in Fe and

BGD
8, 7953–8000, 2011

also the inner part of the test wall shows a Fe rich spot. These Fe rich phases are absent in the specimens which have been treated with an oxidative cleaning procedure (Figs. 6 and 7) except in a pore of the specimen from 465 m water depth (Fig. 7). All Ca distributions show strongly heterogenous patterns. These patterns can be recognized on secondary-electron (SE) and backscattered-electron (BSE) images, too (Fig. 8). These images have been made after the mappings. The BSE images show that these structures look like some kind of porous bands in the test walls where the Ca maps show higher count rates.

3.3 Redox sensitive elements in tests of *B. spissa*

The measured Mn/Ca and Fe/Ca ratios for the Ecrm752, a limestone prepared under laboratory conditions (Greaves et al., 2008), the OKA calcite grain and the tests of *B. spissa* are listed in Table 5 (ICP-MS), Table 6 (SIMS) and Table 7 (mean SIMS). The Ecrm752 solution was used as internal reference standard for the ICP-MS analyses (mean Mn/Ca = 139.30 µmol mol^{-1}; mean Fe/Ca = 155.28 µmol mol^{-1}). Element ratios for the Ecrm752 showed a sufficiently high reproducibility with standard deviations of 4.02 µmol mol^{-1} (Mn/Ca) and 5.18 µmol mol^{-1} (Fe/Ca) between the different measurements. The Mn/Ca and Fe/Ca ratios for the Ecrm752 have also been determined in an inter laboratory calibration study (Greaves et al., 2008). The data presented in our study are in accordance to the values reported for the the not centrifuged Ecrm752 where the Mn/Ca ratio ranged from 121–147 µmol mol^{-1} and the Fe/Ca ratio ranged from 97–220 µmol mol^{-1} between the different laboratories. The mean element ratios for the Oka calcite grain which was used as cross calibration standard for the SIMS analyses was also determined with ICP-MS (mean Mn/Ca = 4930.33 µmol mol^{-1}; mean Fe/Ca = 541.33 µmol mol^{-1}).

The Mn/Ca and Fe/Ca ratios in tests of *B. spissa* are shown in Fig. 10. The mean ratios from the SIMS spot analyses for single specimens are plotted as well as the ratios from ICP-MS analyses on bulk solutions of several specimens. The ratios of the bulk samples compared to the microanalyses agree in a maximal differences of

BGD
8, 7953–8000, 2011

3–29 % compared to the overall data range between the different sampling sites, although the Mn/Ca ratio from the bulk analysis is a bit elevated compared to the microanalysis result (3.8 µmol mol^{-1} compared to 2.12 µmol mol^{-1}). The Mn/Ca ratios range from 2.12–9.93 µmol mol^{-1} and thus are in general quite low. This falls far below the generally accepted level of test Mn/Ca to prove the absence of diagenetic coatings from 50 µmol mol^{-1} to >150 µmol mol^{-1} (Boyle, 1983; Boyle and Keigwin, 1985, 1986; Delaney, 1990; Ohkouchi et al., 1994). The corresponding Fe/Ca ratios range from 86.99–551.82 µmol mol^{-1}. Both element ratios show an increasing trend towards deeper water depths and higher bottom water oxygenation. The standard deviations between the different SIMS spots on single specimens are generally higher among the specimens from the deeper and better oxygenated sampling locations, too. They range from 0.37–5.91 µmol mol^{-1} for the Mn/Ca and from 23.06–392.98 µmol mol^{-1} for the Fe/Ca ratio. The Mn/Ca and Fe/Ca ratio for an uncleaned specimen of *B. spissa* is also shown in Fig. 10 indicated by a green diamond. Compared to a specimen from the same sampling site treated with oxidative cleaning it shows an elevated Fe/Ca ratio and a slightly reduced Mn/Ca ratio.

3.4 Comparison to pore-water data

The correlation between Mn/Ca ratios in the top cm of the pore water and Mn/Ca in tests of *B. spissa* from the same sampling locations are shown in Fig. 12. The Mn/Ca ratios in *B. spissa* are generally higher at locations where Mn/Ca ratios are higher in the pore-waters.

The Fe concentrations among the pore water profiles of three sampling locations are shown in Fig. 11. The core from the shallowest most oxygen depleted sampling site shows a sharp Fe peak with high Fe concentrations in the top 2 cm of the pore waters. In contrast to this profile the Fe/Ca ratios in tests of *B. spissa* from this location are the lowest found among all samples. The Fe concentration in the pore waters from the deeper sampling locations show a more typical behaviour with increasing concentrations at sediment depths where the Fe reduction starts.

BGD
8, 7953–8000, 2011

4 Discussion

4.1 Chemical test composition of *U. peregrina*

The trace element mappings of *U. peregrina* cross-sections show an iron rich phase which is strongly enriched in different elements. This phase seems to be similar like "coatings" which have been found in the inner chamber walls of *Globigerinoides ruber* (Gehlen et al., 2004). Since this phase is removed after an oxidative cleaning without a reductive cleaning step it is unreasonable that it represents an (oxyhydr)oxide coating. Also the low Mn content shows that it does not consist of manganese carbonate. It has more chemical similarity with cements in tests of several agglutinated foraminifera and the test walls of several allogromiids show a similar chemical composition (Bertram and Cowen, 1998; Gooday et al., 2008).

Elevated Fe concentrations inside the pores also show the presence of the Fe rich lining. Thus in microanalytical techniques like EMP, SIMS or LA-ICP-MS it should be avoided to measure at the porous parts of the test walls, because the inner organic lining, also present in the test pores, shows, partly due to the presence of clay particles, strongly elevated concentrations in several elements, even Mg. Furthermore it should be avoided to measure at the inner test surface and inside the chambers themselves because of the presence of the Fe rich lining and the muddy accumulations inside the chambers.

The element mappings show no hints for ferro-manganese-oxide coatings which is most probably related to the highly reducing conditions in the pore waters at the OMZ off Peru. At least for recent samples a reductive cleaning for chemical analyses seems to be not necessarily required. The comparison of the uncleaned specimens with a specimen treated with an oxidative cleaning shows that the oxidative cleaning removes the contaminant Fe rich phase at the inner surface of the test walls. This hints again that this phase represents more the inner organic lining of the test than a diagenetic coating. Also it proofs the value of the oxidative cleaning for the minimization of contaminations inside foraminiferal tests.

BGD
8, 7953–8000, 2011

4.2 Chemical composition of *B. spissa* tests

An iron rich phase present in the uncleaned specimens of *U. peregrina* and *B. spissa* seems to be absent in specimens of *B. spissa* treated with an oxidative cleaning procedure. To minimize contaminations during the microanalysis of foraminiferal tests it is absolutely necessary to use an oxidative cleaning step during sample preparation. But even after intense oxidative cleaning there are still contaminations left inside the test pores. Thus it should be avoided to measure parts of the tests where pores are present. This might be especially complicated during the analyses of foraminifera with a high pore-density with laser ablation due to the spot diameter (50–80 µm) required for low concentration measurements on Q-ICP-MS. Nevertheless the test walls seem to be contamination free after the oxidative cleaning where no pores are present. The element/Ca ratios measured with SIMS in the tests of the cleaned *B. spissa* specimens should therefore represent the element/Ca ratios of the test calcite. This might be more complicated during the presence of diagenetic oxyhdroxide or Mn carbonate coatings. In this case EMP mappings should be used as pre-investigation to locate these coatings and for identification of the measurement spots in the contamination free areas. Additionally the effectivity of a reductive cleaning treatment could be analysed by EMP mapping by comparing cleaned and uncleaned specimens.

The strong Mg-bends present in *U. peregrina* are not visible in *B. spissa*. This might be explained by the fact that bolivinidae construct their tests in a monolamellar concept without a second phase of calcite between the different layers (Sliter, 1974).

Still enigmatic remain the heterogeneous patterns in Ca distribution. The Ca count rates are higher where these holey structures are visuable in the BSE images. This appears to be puzzling because in this case the Ca concentration would be higher at spots of low density. Thus it is probable that the higher Ca count rates in the holey structures are rather artifacts due to topography related analytical problems with. It seems likely that the high energetic X-ray beam pitted the surface of the sample by burning more volatile parts of the test wall.

BGD
8, 7953–8000, 2011

4.3 Redox sensitive elements in pore waters and *B. spissa*

4.3.1 Mn/Ca ratios

Reductive dissolution of reactive Mn (oxyhydr)oxides in the surface sediments drive the Mn flux across the benthic boundary (Froelich et al., 1987; Burdige et al., 1993; Pakhomova et al., 2007; Noffke et al., 2011; Scholz et al., 2011). The Mn concentrations and thus the Mn/Ca ratios are relatively low in the pore waters from the OMZ off Peru since most of the Mn delivered to the OMZ is already reduced in the water column (Böning et al., 2004; Scholz et al., 2011).The Mn/Ca ratios in tests of *B. spissa* and the Mn concentrations in the top cm of the pore waters are generally relatively low and show an increasing trend with higher bottom water oxygenation. At a first glance these results appear to be confusing because usually solid MnO_2 is rapidly reduced to soluble Mn^{2+} in oxygen depleted pore waters. Thus it is expectable that Mn concentrations are elevated in the top pore water interval when bottom water oxygen is depleted. Indeed the permanently anoxic OMZ off Peru causes MnO_2 reduction to occur already in the water column, and hence only minor amounts of particulate bound Mn arrive at the seafloor (Böning et al., 2004). Even if the pore water conditions are highly reducing only little Mn can be mobilised due to the absence of particulate MnO_2. At deeper water depths below the OMZ the oxygen concentration starts to rise again and soluble Mn^{2+} can be oxygenated to MnO_2 which again settles down to the seafloor. Thus at the deeper sampling locations the Mn concentrations in the top pore water intervals can be higher due to the higher reservoir in particulate MnO_2 although (or in this case because) the bottom water oxygen concentrations are higher. As already mentioned even the Mn/Ca ratios in *B. spissa* reflect these conditions. These results can be used to interpret downcore profiles of Mn/Ca ratios in benthic foraminifera from the Peruvian OMZ. Elevated Mn/Ca ratios would hint to higher oxygen concentrations during this time due to a higher MnO_2 flux to the ground.

BGD
8, 7953–8000, 2011

The Mn/Ca and the Fe/Ca ratios both obviously show a higher variability in tests of *B. spissa* from habitats with elevated $[O_2]_{BW}$. Infaunal foraminiferal species are able to migrate vertically in the sediments to where food availability and oxygenation meet their individual requirements (Jorissen et al., 1995; Duijnstee, 2003). At higher $[O_2]_{BW}$ and thus a deeper oxygen penetration depth *B. spissa* might be able to migrate deeper into the sediments. In this case individual specimens would be exposed to a wide range of Mn and Fe concentrations in the pore waters among their lifetime. The comparison between the cleaned and the uncleaned specimen from 640 m water depth (M77-1-565/MUC-60) shows that the uncleaned specimen has an elevated Fe/Ca and a slightly reduced Mn/Ca ratio. The elevated Fe/Ca ratio originates most probably from the contamination of that Fe rich phase which could be seen on EMP mappings of the uncleaned *B. spissa* and *U. peregrina* specimens. The slightly lower Mn/Ca ratio might be more a variability in the lattice bound Mn concentrations between different specimens.

4.3.2 Fe/Ca ratios and comparison to pore waters

The Fe pore water profiles show more typical concentration levels as compared to Mn. However, the interpretation of the Fe/Ca ratios in *B. spissa* is complex in this regard because they appear to contradict the trend of the pore water concentrations: the lowest foraminiferal Fe/Ca ratios were found at 465 m water depth, a location with a strong sharp Fe peak in the pore water next to the sediment surface. Note, no living specimens of *B. spissa* were found at this location during sampling time although a very high amount of dead tests was present. At the two other sampling locations where pore water profiles are available (579 and 928 m water depth) living specimens of *B. spissa* could be found during sampling time (Mallon et al., 2011). In the centre of the OMZ *B. spissa* is completely absent (Glock et al., 2011). This suggests that *B. spissa* needs at least trace amounts of oxygen to survive or enough nitrate for denitrification.

A likely scenario, which can explain all observations and facts outlined above is that the habitat only recently turned anoxic causing the death of high numbers of *B.*

BGD
8, 7953–8000, 2011

spissa. The subsurface peak of Fe is likely the result of enhanced Fe-reduction, which formed after a phase of oxygenation and enhanced deposition and/or precipitation of Fe-(oxyhydr)oxides at the sediment surface (Scholz et al., 2011). The sampling site at 465 m water depth is located at the lower boundary of the Peruvian OMZ where ingression of oxygenated water masses occurs episodically. Overall, this means that the Fe mobilisation in the pore waters most likely started only after their death so that the Fe could not be incorporated into the test calcite anymore. Also the habitat either experienced a long phase of oxygenation short time before or these phases have to occur periodically over, because high amounts of dead *B. spissa* have been found in the top 3 cm of the sediment. These phases of oxygenation have to be at least long enough for *B. spissa* to survive and build up relative big sociations.

Some iron pore water profiles from different water depth at 11° S (taken from Scholz et al., 2011) are shown in Fig. 13. The shallowest sampling site at the lower boundary of the OMZ (85 m) shows relatively high Fe concentrations in the pore water which might be partly due to an increased supply of detrital (oxyhydr)oxides from the continent (Suits and Arthur, 2000; Scholz et al., 2011). Very likely another portion of iron supply at this station has been delivered through lateral transport in the water column from deeper sediments in the center of the OMZ and the dissolved Fe is re-oxidized and deposited at the shallower shelf in times of shelf oxygenation. This Fe pool is reduced again when anoxic conditions re-establish and leads to the relatively high pore-water concentrations compared to the stations in the center of the OMZ (Noffke et al., 2011; Scholz et al., 2011). The pore water profiles in the permanent anoxic part of the OMZ (319 m, 410 m) show relatively low Fe concentrations while the peak at 465 m water depth again is similar to this one at 85 m although it is not distinctive. It might be that dissolved Fe has been delivered here by lateral transport in the water column from sediments at the centre of the OMZ. In this case as already mentioned oxygen supply from the deeper water masses might have lead to re-oxygenation of the dissolved iron. The new formed (oxyhydr)oxides are reduced again when anoxic conditions re-establish at this sampling site which again leads to these relatively high Fe concentrations in the

BGD
8, 7953–8000, 2011

shallow pore-water. The trend of the higher pore water concentrations with increasing water depth at the deeper stations (579 m, 928 m) reflects the transition from sulphate reduction to iron reduction. This trend is reflected by the Fe/Ca ratios in *B. spissa*, too.

5 Conclusions

An iron rich phase has been found at the inner surface of the test walls and also in the pores of several specimens of *U. peregrina*. This phase also is enriched in Al, Si, P and S and it could be efficiently removed from the walls with an oxidative cleaning procedure. A similar phase enriched in Fe could be removed from the inner parts of the test walls of *B. spissa* with oxidative cleaning, too. Nevertheless, even after the oxidative cleaning Fe was still enriched in the pores. Thus an oxidative cleaning procedure is essential to minimize the influences of non-lattice bound signatures during the determination of element/Ca ratios even for microanalytical methods. Furthermore it should be avoided to measure at parts of the test wall where pores are present. None of the EMP maps shows any hint for diagenetic coatings. Therefore a reductive cleaning for the determination of element/Ca ratios was not necessary. For minimisation of the whole procedure blank and the loss of sample material it is a good choice to avoid unnecessary cleaning steps.

A comparison of Fe/Ca and Mn/Ca ratios in tests of *B. spissa* determined with SIMS and ICP-MS showed that the results of these two techniques agree in a maximal differences of 3–29 % compared to the overall data range between the different sampling sites. The low Mn/Ca ratios are in the same magnitude as in the pore waters. The low Mn concentrations in the pore waters originate most propably from the strong oxygen depletion in the water column of the Peruvian OMZ. Most MnO_2 is already reduced in the water column and does not settle down to the sediments. The Mn/Ca ratios in *B. spissa* correlate with the Mn/Ca ration in the top cm of the pore water. Thus Mn/Ca ratios in benthic foraminifera from the Peruvian OMZ could be used to trace the amount of oxygen depletion in the OMZ. In downcore proxy application higher Mn/Ca ratios would

BGD
8, 7953–8000, 2011

indicate a better oxygenation because more MnO_2 settles down to the seafloor, being remobilised in the pore waters. Several observations at a strongly oxygen depleted location, like low Fe/Ca ratios in *B. spissa*, a strong sharp Fe peak in the top interval of the pore water and the presence of a high amount of dead but no living specimens of *B. spissa*, hint that this site just recently turned anoxic. Therefore the Fe flux out of the sediment started after the death of *B. spissa* at this site. The sharp peak also might hint that ironoxides, that precipitated in a period of higher oxygen supply, just started to get remobilised when the sediment turned anoxic again.

The fact that the Fe/Ca ratios in *B. spissa* reflect not always the pore water conditions might complicate approaches in paleoreconstruction in contrast to the Mn/Ca ratios which seem to be a very promising tool. Nevertheless, future downcore studies will show the value of these proxies in paleoreconstruction.

Acknowledgements. We thank Anna Noffke, Florian Scholz, Bettina Domeyer, Meike Dibbern, and Renate Ebinghaus for performing pore-water trace element measurements, Mario Thöner for support in the operation of the EMP at the IFM-Geomar in Kiel and Ilona Schäpan for support in the SIMS measurements at the GFZ in Potsdam. Ed Hathorne is acknowledged for providing of the OKA and ECRM 752 calibration standards to this work. The scientific party on R/V *METEOR* cruise M77 is acknowledged for their general support and advice in multicorer operation and sampling. The "Deutsche Forschungsgemeinschaft, (DFG)" provided funding through SFB 754 "Climate – Biogeochemistry Interactions in the Tropical Ocean".

References

Allison, N. and Austin, W. E. N.: The potential of ion microprobe analysis in detecting geochemical variations across individual foraminifera tests, Geochem. Geophy. Geosy., 4(2), 8403, doi:10.1029/2002GC000430, 2003.

Barker, S., Greaves, M., and Elderfield, H.: A study of cleaning procedures used for foraminiferal Mg/Ca paleothermometry, Geochem. Geophy. Geosy., 4(9), 8407, doi:10.1029/2003GC000559, 2003.

Bertram, C. J., Elderfield, H., Shackleton, N. J., and MacDonald, J. A.: Cadmium/calcium and

BGD
8, 7953–8000, 2011

carbon isotope reconstructions of the glacial northeast Atlantic Ocean, Paleoceanography, 10(3), 563–578, 1995.
Bertram, M. A. and Cowen, J. P.: Biomineralization in Agglutinating Foraminifera: An Analytical SEM Investigation of External Wall Composition in Three Small Test Forms, Aquat. Geochem., 4, 455–468, 1998.
Bice, K. L., Layne, G. D., and Dahl, K.: Application of secondary ion mass spectrometry to the determination of Mg/Ca in rare, delicate, or altered planktonic foraminifera: Examples from the Holocene, Paleogene, and Cretaceous, Geochem. Geophy. Geosy., 6, Q12P07, doi:10.1029/2005GC000974, 2005.
Boyle, E. A.: Cadmium, zinc, copper and barium in foraminifera tests, Earth Planet Sc. Lett., 53, 11–35, 1981.
Boyle, E. A.: Manganese carbonate overgrowths on foraminifera tests, Geochim. Cosmochim. Ac., 47, 1815–1819, 1983.
Boyle, E. A.: Cadmium: Chemical tracer of deep-water paleoceanography, Paleoceanography, 3, 471–489, 1988.
Boyle, E. A. and Keigwin, L. D.: Comparison of Atlantic and Pacific paleochemical records for the last 215,000 years: Changes in deep ocean circulation and chemical inventories, Earth Planet. Sc. Lett., 76, 135–150, 1985.
Burdige, D. J.: The biogeochemistry of manganese and iron reduction in marine sediments, Earth-Sci. Rev., 35, 249–284, 1993.
Came, R. E., Oppo, D. W., and Curry, W. B.: Atlantic Ocean circulation during the Younger Dryas: Insights from a new Cd/Ca record from the western subtropical South Atlantic, Paleoceanography, 18(4), 1086, doi:10.1029/2003PA000888, 2003.
Delaney, M. L.: Miocene benthic foraminiferal Cd/Ca records: South Atlantic and western Equatorial Pacific, Paleoceanography, 5, 743–760, 1990.
Eggins, S., De Deckker, P., and Marshall, J.: Mg/Ca variation in planktonic foraminifera tests: Implications for reconstructing paleoseawater temperature and habitat migration, Earth Planet. Sc. Lett., 6694, 1–16, 2003.
Eggins, S., Sadekov, A., and De Deckker, P.: Modulation and daily banding of Mg/Ca in Orbulina universa tests by symbiont photosynthesis and respiration: A complication for seawater thermometry?, Earth Planet. Sc. Lett., 225, 411–419, 2004.
Elderfield, H. and Ganssen, G.: Past temperature and $\delta^{18}O$ of surface ocean waters inferred from foraminiferal Mg/Ca ratios, Nature, 405, 442–445, 2000.

BGD
8, 7953–8000, 2011

Erez, J.: The source of ions for biomineralization in foraminifera and their implications for paleoceanographic proxies, in: Biomineralization: Mineralogical Society of America, edited by: Dove, P. M., De Yoreo, J. J., and Weiner, S., Washington, D. C., 115–149, 2003.

Fhlaithearta, S. N., Reichart, G.-J., Jorissen, F. J., Fontanier, C., Rehling, E. J., Thomson, J., and De Lange, G. J.: Reconstructing the seafloor environment during sapropel formation using benthic foraminiferal trace metals, stable isotopes, and sediment composition, Paleoceanography, 25, PA4225, doi:10.1029/2009PA001869, 2010.

Foster, G. L.: Seawater pH, pCO_2 and $[CO_3^{2-}]$ variations in the Caribbean Sea over the last 130 kyr: a boron isotope and B/Ca study of planktic foraminifera, Earth Planet. Sc. Lett., 271, 254–266, 2008.

Froelich, P. N., Klinkhammer, G. P., Bender, M. L., Luedtke, N. A., Heath, G. R., Cullen, D., Dauphin, P., Hammond, D., Hartman, B., and Maynard, V.: Early oxidation of organic matter in pelagic sediments of the eastern equatorial Atlantic: suboxic diagenesis, Geochim. Cosmochim. Ac., 43, 1075–1090, 1987.

Gaetani, G. A. and Cohen, A. L.: Element partitioning during precipitation of aragonite from seawater: A framework for understanding paleoproxies, Geochim. Cosmochim. Ac., 70, 4117–4137, 2006.

Gehlen, M., Bassinot, F., Beck, L., and Khodja, H.: Trace element cartography of *Globigerinoides ruber* shells using particle-induced X-ray emission, Geochem. Geophy. Geosy., 5(12), Q12D12, doi:10.1029/2004GC000822, 2004.

Glock, N., Eisenhauer, A., Milker, Y., Liebetrau, V., Schönfeld, J., Mallon, J., Sommer, S., and Hensen, C.: Environmental influences on the pore-density in tests of *Bolivina spissa*, J. Foramin. Res., 41, 22–32, 2011.

Gooday, A. J., Todo, Y., Uematsu, K., and Kitazato, H.: New organic- walled Foraminifera (Protista) from the ocean's deepest point, the Challenger Deep (western Pacific Ocean), Zool. Journ. of the Linn. Soc., 153, 399–423, 2008.

Greaves, M., Caillon, N., Rebaubier, H., Bartoli, G., Bohaty, S., Cacho, I., Clarke, L., Cooper, M., Daunt, C., Delaney, M., deMenocal, P., Datton, A., and Eggins, S.: Interlaboratory comparison of calibration standards for foraminiferal Mg/Ca thermometry, Geochem. Geophy. Geosy., 9(8), Q08010, doi:10.1029/2008GC001974, 2008.

Haley, B. A. and Klinkhammer, G. P.: Development of a flow-through system for cleaning and dissolving foraminiferal tests, Chem. Geol., 185, 51–69, 2002.

Haley, B. A., Klinkhammer, G. P., and Mix, A. C.: Revisiting the rare earth elements in

BGD
8, 7953–8000, 2011

foraminiferal tests, Earth Planet. Sc. Lett., 239, 79–97, 2005.
Hall, J. M. and Chan, L.-H.: Ba/Ca in *Neogloboquadrina pachyderma* as an indicator of deglacial meltwater discharge into the western Arctic Ocean, Paleoceanography, 19, 9 pp., doi:10.1029/2004PA001028, 2004a.
Hall, J. M. and Chan, L.-H.: Ba/Ca in benthic foraminifera: Thermocline and middepth circulation in the North Atlantic during the last glaciations, Paleoceanography, 19, 13 pp., doi:10.1029/2003PA000910, 2004b.
Harding, D. J., Arden, J. W., and Rickaby, R. E. M.: A method for precise analysis of trace element/calcium ratios in carbonate samples using quadrupole inductively coupled plasma mass spectrometry, Geochem. Geophy. Geosy., 7, Q06003, doi:10.1029/2005GC001093, 2006.
Hastings, D. W., Emerson, S., Erez, J., and Nelson, B. K.: Vanadium incorporation in foraminiferal calcite as a paleotracer for seawater vanadium concentrations, Geochim. Cosmochim. Ac., 19, 3701–3715, 1996a.
Hastings, D. W., Emerson, S. E., and Nelson, B.: Determination of picogram quantities of vanadium in foraminiferal calcite and seawater by isotope dilution inductively coupled plasma mass spectrometrwy ith electrothermavla porization, Anal. Chem., 68, 371–378, 1996b.
Hastings, D. W., Emerson, S. R., and Mix, A. C.: Vanadium in foraminiferal calcite as a tracer for changes in the areal extent of reducing sediments, Paleoceanography, 11(6), 665–678, 1996c.
Hastings, D. W., Russell, A. D., and Emerson, S. R.: Foraminiferal magnesium in Globeriginoides sacculifer as a paleotemperature proxy, Paleoceanography, 13(2), 161–169, 1998.
Hathorne, E. C., Alard, O., James, R. H., and Rogers, N. W.: Determination of intratest variability of trace elements in foraminifera by laser ablation inductively coupled plasma-mass spectrometry, Geochem. Geophy. Geosy., 4(12), 8408, doi:10.1029/2003GC000539, 2003.
Kasemann, S. A., Schmitt, D. N., Bijma, J., and Foster, G. L.: *In situ* boron isotope analysis in marine carbonates and its application for foraminifera and palaeo-pH, Chem. Geol., 260, 138–147, 2009.
Kunioka, D., Shirai, K., Takahata, N., Sano, Y., Toyofuku, T., and Ujiie, Y.: Microdistribution of Mg/Ca, Sr/Ca and Ba/Ca ratios in Pulleniatina obliquiloculata test by using NanoSIMS: implication for the vital effect mechanism, Geochem. Geophy. Geosy., 7, Q12P20, doi:10.1029/2006GC001280, 2006.
Lear, C. H., Rosenthal, Y., and Slowey, N.: Benthic foraminiferal Mg/Ca-paleothermometry: A

BGD
8, 7953–8000, 2011

revised coretop calibration, Geochim. Cosmochim. Ac., 66(19), 3375–3387, 2002.
Lea, D. W.: Trace elements in foraminiferal calcite Modern Foraminifera, edited by: Sen Gupta, B. K., Kluwer Academic Publishers, New York, Boston, Dordrecht, London, Moscow, 201–216, 2003.
Lea, D. W. and Boyle, E. A.: Barium content of benthic foraminifera controlled by bottom-water composition, Nature, 338, 751–753, 1989.
Lea, D. W. and Boyle, E. A.: Foraminiferal reconstruction of barium distributions in water masses of the glacial oceans, Paleoceanography, 5, 719–742, 1990a.
Lea, D. W. and Boyle, E. A.: A 210,000-year record of barium variability in the deep northwest Atlantic Ocean, Nature, 347, 269–272, 1990b.
Lea, D. W. and Boyle, E. A.: Barium in planktonic foraminifera, Geochim. Cosmochim. Ac., 55, 3321–3331, 1991.
Lea, D. W. and Spero, H. J.: Experimental determination of barium uptake in shells of the planktonic foraminifera Orbulina universa at 22°C, Geochim. Cosmochim. Ac., 56, 2673–2680, 1992.
Lea, D. W. and Spero, H. J.: Assessing the reliability of paleochemical tracers: Barium uptake in the shells of planktonic foraminifera, Paleoceanography, 9, 445–452, 1994.
Lea, D. W., Mashiotta, T. A., and Spero, H. J.: Controls on magnesium and strontium uptake in planktonic foraminifera determined by live culturing, Geochim. Cosmochim. Ac., 63, 2369–2379, 1999.
Mallon, J., Glock, N., and Schönfeld, J.: The response of benthic foraminifera to low-oxygen conditions of the Peruvian oxygen minimum zone, in: ANOXIA: Evidence for eukaryote survival and paleontological strategies, edited by: Altenbach, A. V., Bernhard, J. M., and Seckbach, J., Springer, in press, 2011.
Marchitto, T. M.: Precise multielemental ratios in small foraminiferal samples determined by sector field ICP-MS, Geochem. Geophy. Geosy., 7, Q05P13, doi:10.1029/2005GC001018, 2006.
Marchitto Jr., T. M., Curry, W. B., and Oppo, D. W.: Zinc concentrations in benthic foraminifera reflect seawater chemistry, Paleoceanography, 15(3), 299–306, 2000.
Martin, P. A. and Lea, D. W.: Comparison of water mass changes in the deep tropical Atlantic derived from Cd/Ca and carbon isotope records: Implications for changing Ba composition of deep Atlantic water masses, Paleoceanography, 13, 572–585, 1998.
Munsel, D., Kramar, U., Dissard, D., Nehrke, G., Berner, Z., Bijma, J., Reichart, G.-J.,

BGD
8, 7953–8000, 2011

and Neumann, T.: Heavy metal incorporation in foraminiferal calcite: results from multi-element enrichment culture experiments with Ammonia tepida, Biogeosciences, 7, 2339–2350, doi:10.5194/bg-7-2339-2010, 2010.

Ni, Y., Foster, G. L., Bailey, T., Elliott, T., Schmidt, D. N., Pearson, P., Haley, B., and Coath, C.: A core top assessment of proxies for the ocean carbonate system in surface dwelling Foraminifers, Paleoceanography, 22(3), 14 pp., 2007.

Noffke, A., Hensen, C., Sommer, S., Scholz, F., Bohlen, L., Mosch, T., and Wallmann, K.: The benthic diagenetic phosphorus and iron source across the Peruvian oxygen minimum zone, Limnol. Oceanogr., submitted, 2011.

Nürnberg, D.: Magnesium in tests of *Neogloboquadrina pachyderma* sinistral from high northern and southern latitudes, J. Foramin. Res., 25, 350–368, 1995.

Nürnberg, D., Bijma, J., and Hemleben, C.: Assessing the reliability of magnesium in foraminiferal calcite as a proxy for water mass temperatures, Geochim. Cosmochim. Ac., 60(5), 803–814, 1996.

Ohkouchi, N., Kawahata, H., Murayama, M., Ohkada, M., Nakamura, T., and Taira, A.: Was deep water formed in the North Pacific during the Late Quaternary? Cadmium evidence from the northwest Pacific, Earth Planet. Sc. Lett., 124, 185–194, 1994.

Pakhomova, S. V., Hall, P. O. J., Kononets, M. Y., Rozanov, A. G., Tengberg, A., and Vershinin, A. V.: Fluxes of iron and manganese across the sediment-water interface under various redox conditions, Mar. Chem., 107, 319–331, 2007.

Palmer, M. R. and Pearson, P. N.: A 23,000-year record of surface water pH and pCO_2 in the western equatorial Pacific Ocean, Science, 300, 480–482, 2003.

Palmer, M. R., Pearson, P. N., and Cobb, S. J.: Reconstructing past ocean pH-depth profiles, Science 282, 1468–1471, 1998.

Pearson, P. N. and Palmer, M. R.: Atmospheric carbon dioxide concentrations over the past 60 million years, Nature, 406, 695–699, 2000.

Pena, L. D., Calvo, E., Cacho, I., Eggins, S., and Pelejero, C.: Identification and removal of Mn-Mg-rich contaminant phases on foraminiferal tests: Implications for Mg/Ca past temperature reconstructions, Geochem. Geophy. Geosy., 6, Q09P02, doi:10.1029/2005GC000930, 2005.

Pena, L. D., Cacho, I., Calvo, E., Pelejero, C., Eggins, S., and Sadekov, A.: Characterization of contaminant phases in foraminifera carbonates by electron microprobe mapping, Geochem. Geophy. Geosy., 9, Q07012, doi:10.1029/2008GC002018, 2007.

BGD
8, 7953–8000, 2011

Rae, J. W. B., Foster, G. L., Schmitt, D. N., and Elliot, T.: Boron isotopes and B/Ca in benthic foraminifera: Proxies for the deep ocean carbonate system, Earth Plane. Sc. Lett., 302, 403–413, 2011.

Reichart, G.-J., Jorissen, Mason, F. P. R. D., and Anschutz, P.: Single foraminiferal test chemistry records the marine environment, Geology, 31, 355–358, 2003.

Rollion-Bard, C. and Erez, J.: Intra-shell boron isotope ratios in the symbiont-bearing benthic foraminiferan Amphistegina lobifera: Implications for δ^{11}B vital effects and paleo-pH reconstructions, Geochim. Cosmochim. Ac., 74, 1530–1536, 2010.

Rollion-Bard, C., Erez, J., and Zilberman, T.: Intra-shell oxygen isotope ratios in the benthic genus Amphistegina and the influence of seawater carbonate chemistry and temperature on this ratio, Geochim. Cosmochim. Ac., 72, 6006–6014, 2008.

Rosenthal, Y., Boyle, E. A., and Slowey, N.: Temperature control on the incorporation of magnesium, strontium, fluorine, and cadmium into benthic foraminiferal shells from Little Bahama Bank: Prospects for thermocline paleoceanography, Geochim. Cosmochim. Ac., 61, 3633–3643, 1997.

Russell, A. D., Emerson, S., Nelson, B., Erez, J., and Lea, D. W.: Uranium in foraminiferal calcite as a recorder of seawater uranium concentrations, Geochim. Cosmochim. Ac., 58(2), 671–681, 1994.

Russell, A. D., Hönisch, B., Spero, H. J., and Lea, D. W.: Effects of seawater carbonate ion concentration and temperature on shell U, Mg, and Sr in cultured planktonic foraminifera, Geochim. Cosmochim. Ac., 68(21), 4347–4361, 2004.

Sadekov, A. Y., Eggins, S. M., and De Deckker, P.: Characterization of Mg/Ca distributions in planktonic foraminifera species by electron microprobe mapping, Geochem. Geophy. Geosy., 6, Q12P06, doi:10.1029/2005GC000973, 2005.

Sano, Y., Shirai, K., Takahata, N., Hirata, T., and Sturchio, N. C.: Nano-SIMS analysis of Mg, Sr, Ba, U in natural calcium carbonate, Anal. Sci., 21, 1091–1097, 2005.

Sanyal, A., Hemming, N. G., Hanson, G. N., and Broecker, W.: Evidence for a higher pH in the glacial ocean from boron isotopes in foraminifera, Nature, 373, 234–236, 1995.

Sanyal, A., Bijma, J., Spero, H. J., and Lea, D.: Empirical relationship between pH and the boron isotopic composition of Globigerinoides sacculifer: implications for the boron isotope paleo-pH proxy, Paleoceanography, 16(5), 515–519, 2001.

Scholz, F., Hensen, C., Noffke, A., Rhode, A., and Wallmann, K.: Early diagenesis of redox-sensitive trace metals in the Peru upwelling area – response to ENSO-related oxygen

BGD

8, 7953–8000, 2011

fluctuations in the water column, Geochim. Cosmochim. Ac., submitted, 2011.
Sliter, W. V.: Test ultrastructure of some living benthic foraminifers: Lethaia, 7, 5–16, 1974.
Spivack, A. J., You, C.-F., and Smith, H. J.: Foraminiferal boron isotope ratios as a proxy for surface ocean pH over the past 21 Myr, Nature, 363, 149–151, 1993.
Suits, N. S. and Arthur, M. A.: Sulfur diagenesis and partitioning in Holocene Peru shelf and upper slope sediments, Chem. Geol., 163, 219–234, 2000.
Toyofuku, T. and Kitazato, H.: Micromapping of Mg/Ca values in cultured specimens of the high-magnesium benthic foraminifera, Geochem. Geophy. Geosy., 6, Q11P05, doi:10.1029/2005GC000961, 2005.
Wu, G. and Hillaire-Marcel, C.: Application of LP-ICP-MS to benthic foraminifers, Geochim. Cosmochim. Ac., 59, 409–414, doi:10.1016/0016-7037(94)00370-2, 1995.
Yu, J., Day, J., Greaves, M., and Elderfield, H.: Determination of multiple element/calcium ratios in foraminiferal calcite by quadrupole ICP-MS, Geochem. Geophy. Geosy., 6, Q08P01, doi:10.1029/2005GC000964, 2005.
Yu, J., Elderfield, H., Greaves, M., and Day, J.: Preferential dissolution of benthic foraminiferal calcite during laboratory reductive cleaning, Geochem. Geophy. Geosy. 8, 17, doi:10.1029/2006GC001571, 2007.
Yu, J., Elderfield, H., Jin, Z., and Booth, L.: A strong temperature effect on U/Ca in planktonic foraminiferal carbonates, Geochim. Cosmochim. Ac., 72, 4988–5000, 2008.

BGD
8, 7953–8000, 2011

Table 1. Sampling sites. $[O_2]_{BW}$ taken from Glock et al. (2011).

Site	Longitude (W)	Latitude (S)	Water depth (m)	$[O_2]_{BW}$ (µmol l^{-1})
M77/1-421/MUC-13	75°34.82′	15°11.38′	519	–
M77/1-455/MUC-21	78°19.23′	11°00.00′	465	2.42
M77/1-487/MUC-39	78°23.17′	11°00.00′	579	3.7
M77/1-565/MUC-60	78°21.40′	11°08.00′	640	8.17
M77/1-604/MUC-74	78°22.42′	11°17.96′	878	34.23
M77/1-445/MUC-15	78°30.02′	11°00.00′	928	36.77

BGD
8, 7953–8000, 2011

Table 2. Spectrometer crystals used at the EMP for different elements.

Element	Crystal	Element	Crystal	Element	Crystal
Ca	PETJ	Ba	PETJ	S	PETH
Mg	TAPH	Mn	LIFH	Si	TAP
Fe	LIFH	P	PETH	Al	TAPH

BGD
8, 7953–8000, 2011

Table 3. Operation conditions for Agilent 7500cx.

	value/description
RF power	1500 W
Nebulizer	PFA (100 µl min^{-1}, self aspirating)
Spray chamber	Glass (cooled to 2 °C)
Autosampler	Cetac ASX 100
Uptake rate (µl min^{-1})	100
Washout time (s)	90
Uptake time (s)	30
Argon plasma gas flow rate (l min^{-1})	15
Argon auxiliary gas flow rate (l min^{-1})	0.2–0.3
Argon nebulizer gas flow rate (l min^{-1})	0.8–0.9
Sample cone	Nickel (Agilent)
Skimmer cone	Nickel
CeO/Ce and Ba^{2+}/Ba^{+} ratios	<2.5 %

BGD
8, 7953–8000, 2011

Table 4. Element concentration for the different standard rows used for ICP-MS.

Standard	Ca (ppm)	Fe (ppt)	Mn (ppt)
Row 1 std 1	10	150	5
Row 1 std 2	10	250	10
Row 1 std 3	10	500	15
Row 1 std 4	10	1000	50
Row 1 std 5	10	3000	100
Row 1 std 6	10	5000	150
Row 2 std 1	10	0	10 000
Row 2 std 2	10	0	20 000
Row 2 std 3	10	0	50 000
Row 2 std 4	10	0	75 000
Row 2 std 5	10	0	100 000
Row 3 std 1	10	0	0
Row 3 std 2	50	0	0
Row 3 std 3	100	0	0
Row 3 std 4	200	0	0

BGD
8, 7953–8000, 2011

Table 5. Element/Ca ratios for different samples determined by ICP-MS.

Material	Mn/Ca (μmol mol^{-1})	1σ (μmol mol^{-1})	Fe/Ca (μmol mol^{-1})	1σ (μmol mol^{-1})
Ecrm752	148.30	10.7	150.1	9.8
Ecrm752	138.20	2.8	150.1	8.0
Ecrm752	137.70	2.1	150.3	7.9
Ecrm752	137.80	1.5	157.3	3.5
Ecrm752	138.30	1.4	157.1	4.5
Ecrm752	138.30	3.7	159.0	5.1
Ecrm752	136.50	1.7	163.1	1.4
Oka	4942.00	57.8	547.7	10.3
Oka	4875.60	181.4	523.1	12.8
Oka	4973.40	54.7	553.2	5.5
B. spissa M77-1-455/MUC-21	3.80	0.06	87.0	3.2
B. spissa M77-1-487/MUC-38			142.0	3.1
B. spissa M77-1-487/MUC-38			157.5	2.1
B. spissa M77-1-565/MUC-60			160.6	3.2
B. spissa M77-1-565/MUC-60			138.1	2.9

BGD
8, 7953–8000, 2011

Table 6. Element/Ca ratios of foraminiferal calcite determined by SIMS.

Material	Mn/Ca (μmol mol^{-1})	1σ (μmol mol^{-1})	Fe/Ca (μmol mol^{-1})	1σ (μmol mol^{-1})
B. spissa M77-1-455/MUC-21	1.679	0.53	108.240	9.7
B. spissa M77-1-455/MUC-21	2.322	0.60	66.860	8.7
B. spissa M77-1-455/MUC-21	2.021	0.61	117.246	10.1
B. spissa M77-1-455/MUC-21	2.463	0.64	111.629	10.2
B. spissa M77-1-487/MUC-38a	5.710	1.01	82.350	8.7
B. spissa M77-1-487/MUC-38a	5.148	0.94	184.964	12.6
B. spissa M77-1-487/MUC-38b	3.482	0.76	227.701	14.3
B. spissa M77-1-487/MUC-38b	6.476	1.02	218.407	14.5
B. spissa M77-1-487/MUC-38b	7.463	1.18	119.215	10.7
B. spissa M77-1-565/MUC-60a	2.823	0.69	48.749	6.1
B. spissa M77-1-565/MUC-60a	4.441	0.81	84.088	6.2
B. spissa M77-1-565/MUC-60a	6.198	0.92	164.134	12.3
B. spissa M77-1-565/MUC-60a	5.610	0.88	78.611	8.3
B. spissa M77-1-565/MUC-60b	2.311	0.58	180.360	12.1
B. spissa M77-1-565/MUC-60b	3.510	0.76	269.790	16.1
B. spissa M77-1-565/MUC-60b	2.759	0.62	423.180	18.5
B. spissa M77-1-565/MUC-60b	3.008	0.63	218.280	12.7
B. spissa M77-1-604/MUC-74	5.293	0.89	216.820	13.2
B. spissa M77-1-604/MUC-74	16.590	2.85	984.400	78.8
B. spissa M77-1-445/MUC-15	9.967	1.23	420.510	21.7
B. spissa M77-1-445/MUC-15	5.567	1.04	853.450	30.0
B. spissa M77-1-445/MUC-15	3.142	0.72	72.129	8.3
B. spissa M77-1-445/MUC-15	8.019	1.17	805.800	91.9

BGD
8, 7953–8000, 2011

Table 7. Mean element/Ca ratios in tests of single *B. spissa* specimens determined with SIMS.

Material	Mn/Ca (μmol mol^{-1})	1σ (μmol mol^{-1})	Fe/Ca (μmol mol^{-1})	1σ (μmol mol^{-1})
B. spissa M77-1-455/MUC-21	2.121	0.347	100.990	23.057
B. spissa M77-1-487/MUC-38a	5.148		184.960	
B. spissa M77-1-487/MUC-38b	5.807	2.073	188.440	60.131
B. spissa M77-1-565/MUC-60a	4.771	1.484	93.896	49.334
B. spissa M77-1-565/MUC-60b	2.897	0.500	272.900	106.680
B. spissa M77-1-604/MUC-74	9.933	5.912	551.820	392.980
B. spissa M77-1-445/MUC-15	6.674	2.964	537.970	366.090

BGD
8, 7953–8000, 2011

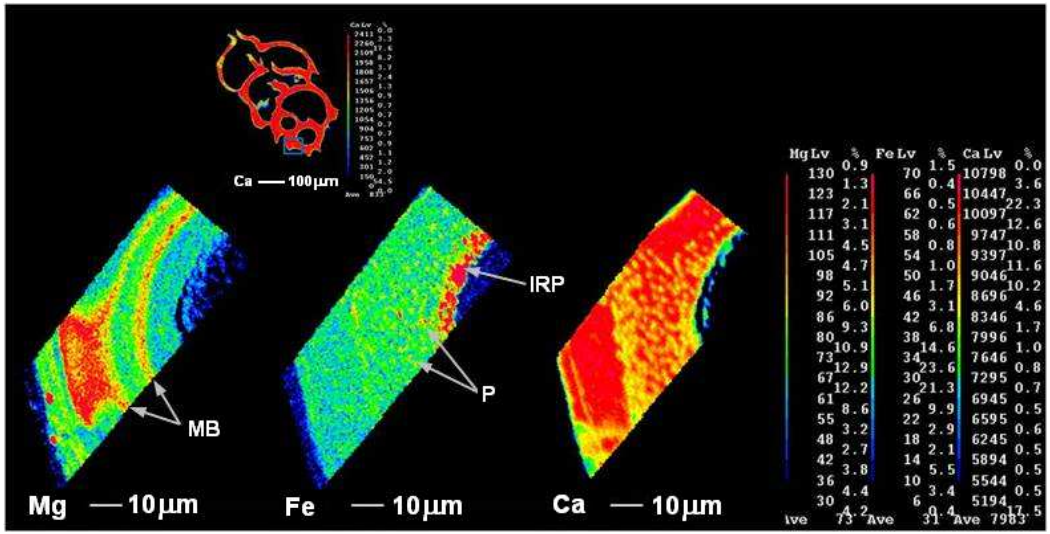

Fig. 1. EMP elemental mappings for an *Uvigerina peregrina* specimen from 519 m water depth (M77-1-421/MUC-13) on an exposed section of the foraminiferal test. Distribution of Ca, Mg and Fe in the foraminiferal test. All intensity values are expressed in counts per second (cps) as shown in the color bars. MB: Mg bands IRP: Fe rich phase at inner test surface and pores (P).

BGD
8, 7953–8000, 2011

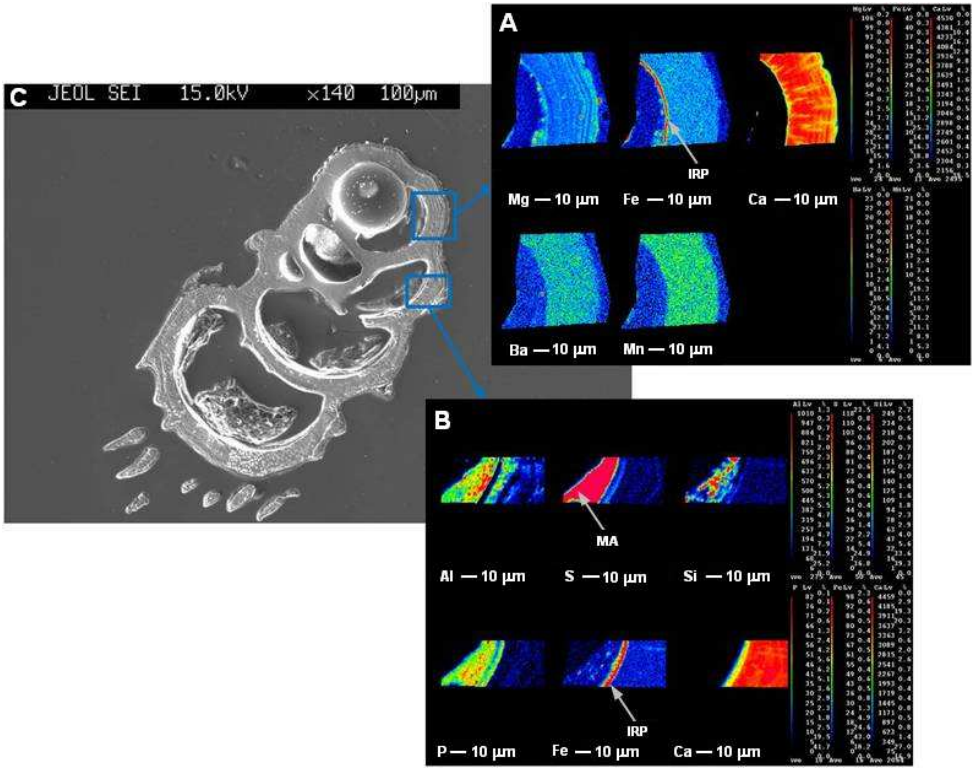

Fig. 2. EMP elemental mappings (**A** and **B**) and secondary electron image **(C)** for an *Uvigerina peregrina* specimen from 579 m water depth (M77-1-487/MUC-39) on an exposed section of the foraminiferal test. Distribution of Ca, Mg, Fe, Ba, Mn, Al, S, Si and P in the foraminiferal test. All intensity values are expressed in counts per second (cps) as shown in the color bars. IRP: Fe rich phase at inner test surface MA: muddy accumulations inside test chambers.

BGD
8, 7953–8000, 2011

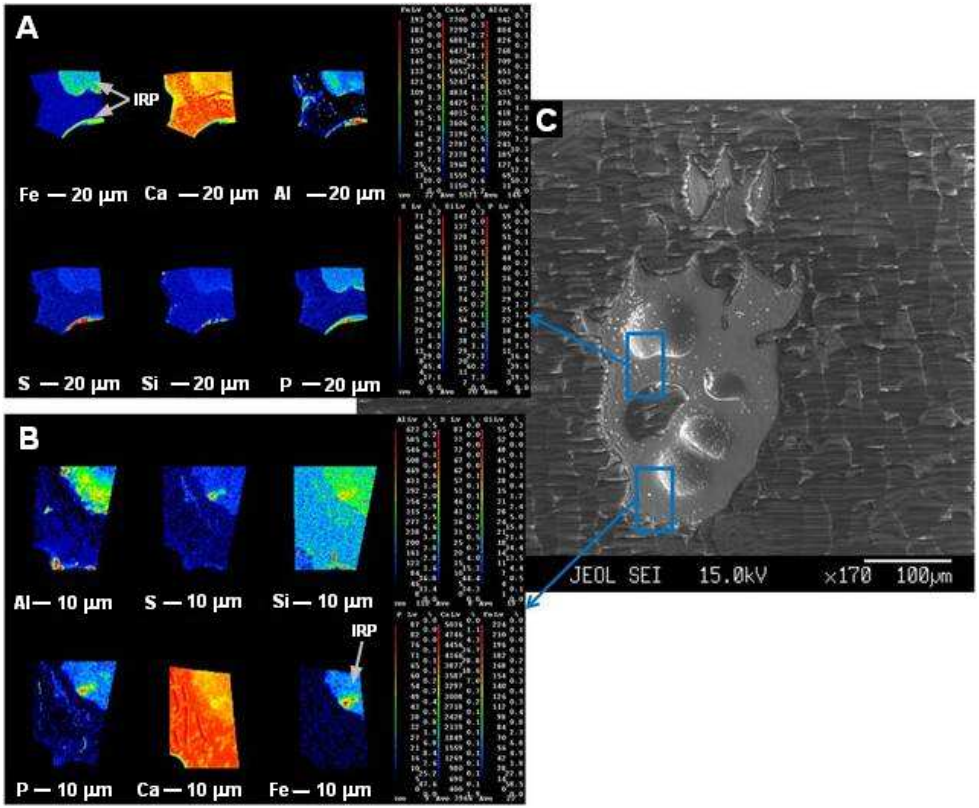

Fig. 3. EMP elemental mappings (**A** and **B**) and secondary electron image **(C)** for an *Uvigerina peregrina* specimen from 579 m water depth (M77-1-487/MUC-39) on an exposed section of the foraminiferal test. Distribution of Ca, Mg, Fe, Ba, Mn, Al, S, Si and P in the foraminiferal test. All intensity values are expressed in counts per second (cps) as shown in the color bars. IRP: Fe rich phase at inner test surface.

BGD
8, 7953–8000, 2011

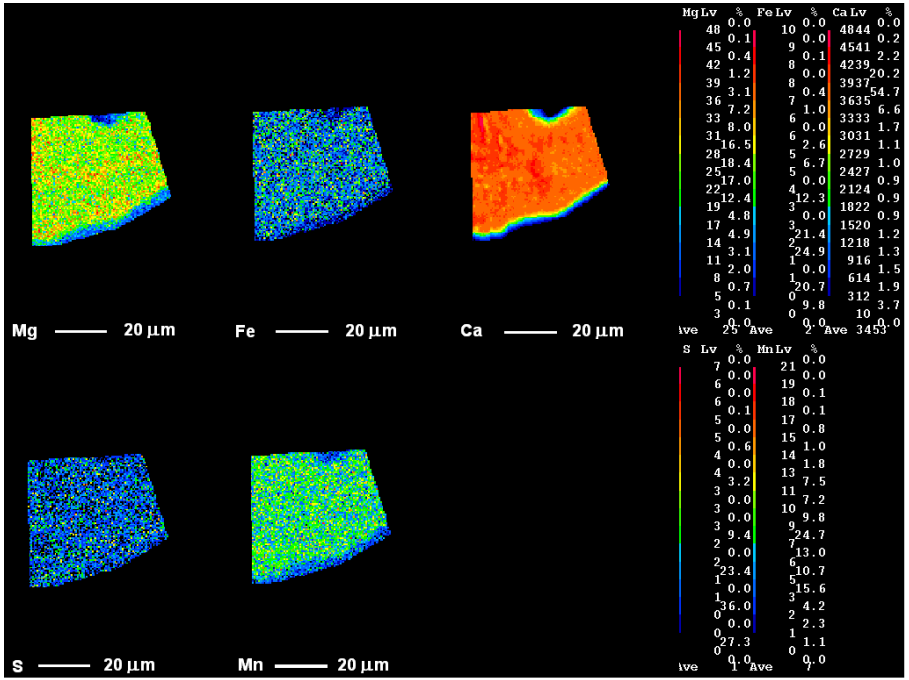

Fig. 4. EMP elemental mapping of a section from an *Uvigerina peregrina* specimen from 640 m water depth (M77-1-565/MUC-60) on an exposed section of the foraminiferal test treated with an oxidative cleaning procedure. Distribution of Mg, Fe, Mn, S and Ca in the foraminiferal test. All intensity values are expressed in counts per second (cps) as shown in the color bars. Note that no contaminant phases are visible in the Fe distribution.

BGD
8, 7953–8000, 2011

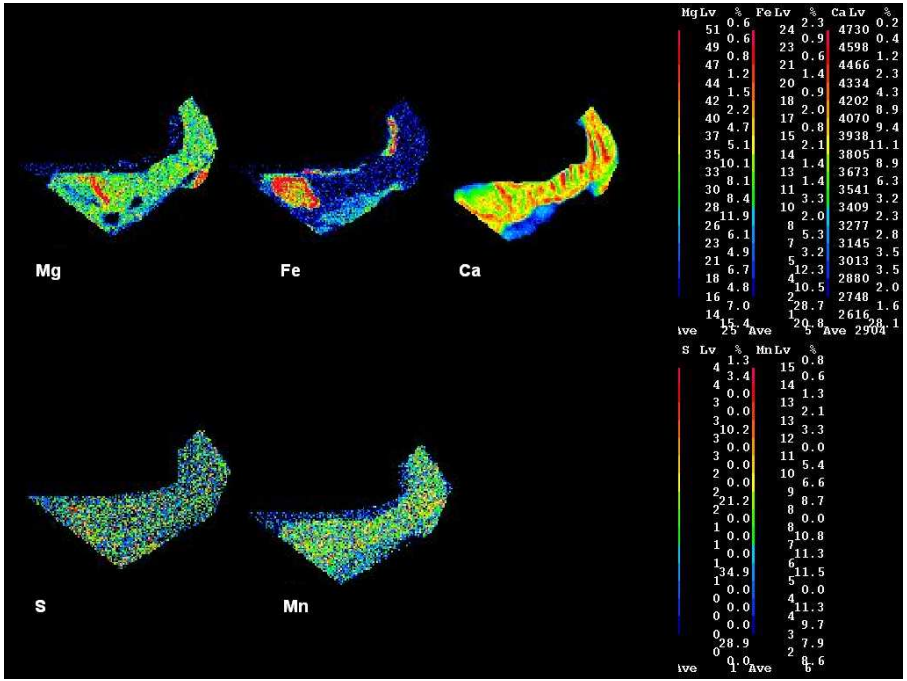

Fig. 5. EMP elemental mapping of a section from an uncleaned *Bolivina spissa* specimen from 640 m water depth (M77-1-565/MUC-60) on an exposed section of the foraminiferal test. Distribution of Mg, Fe, Mn, S and Ca in the foraminiferal test. All intensity values are expressed in counts per second (cps) as shown in the color bars. Note that the Fe distribution shows a contaminant phase a the inner part of the test walls similar like the uncleaned specimens of *U. peregrina*.

BGD
8, 7953–8000, 2011

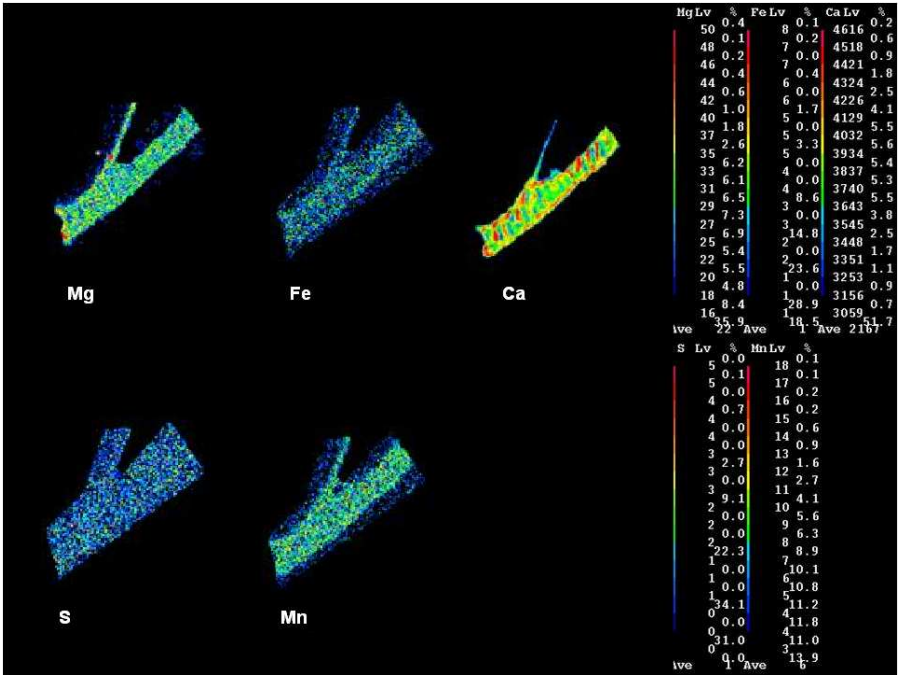

Fig. 6. EMP elemental mapping of a section from a *Bolivina spissa* from 640 m water depth (M77-1-565/MUC-60) on an exposed section of the foraminiferal test specimen treated with an oxidative cleaning procedure. Distribution of Mg, Fe, Mn, S and Ca in the foraminiferal test. All intensity values are expressed in counts per second (cps) as shown in the color bars. Note that no contaminant phases are visible in the Fe distribution.

BGD
8, 7953–8000, 2011

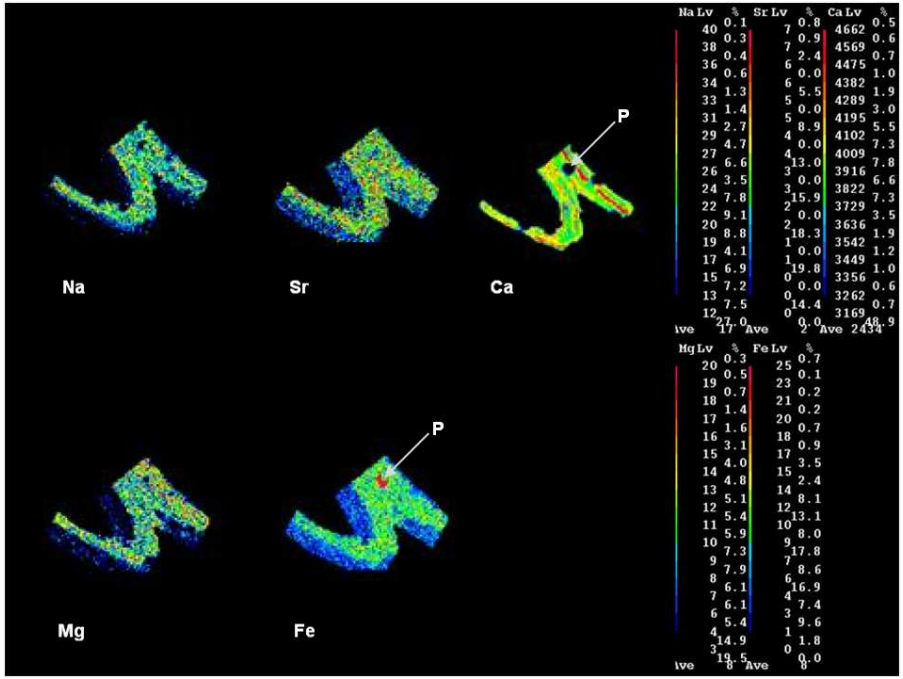

Fig. 7. EMP elemental mapping of a section from a *Bolivina spissa* from 465 m water depth (M77-1-455/MUC-21) on an exposed section of the foraminiferal test specimen treated with an oxidative cleaning procedure. Distribution of Mg, Fe, Mn, S and Ca in the foraminiferal test. All intensity values are expressed in counts per second (cps) as shown in the color bars. Note that no contaminant phases are visible in the Fe distribution except inside a test pore (P).

BGD
8, 7953–8000, 2011

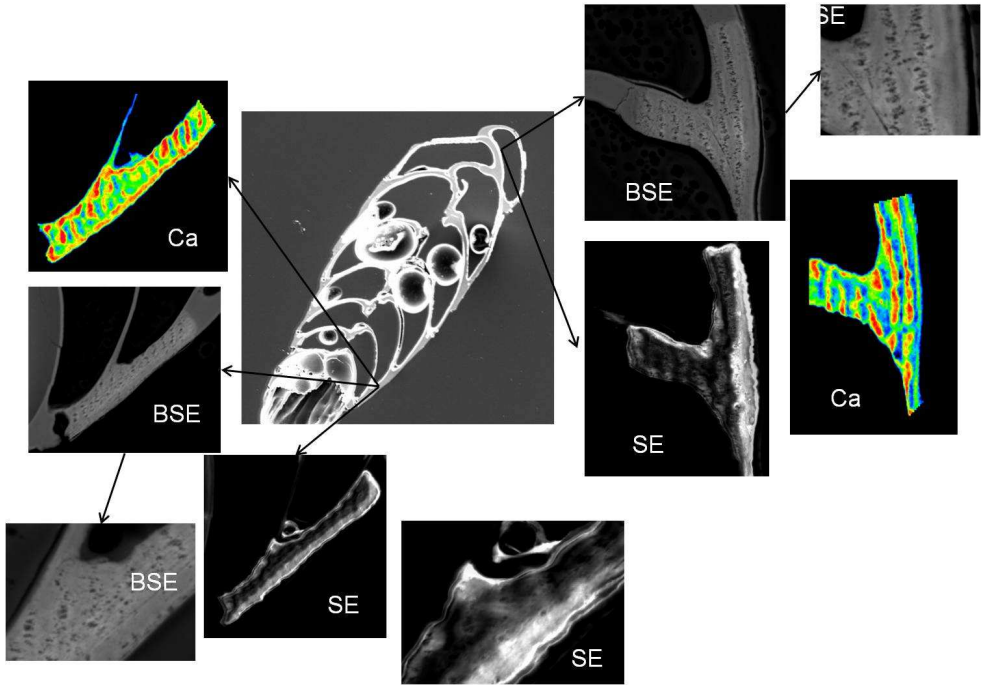

Fig. 8. Cross section of a *Bolivina spissa* specimen from 640 m water depth (M77-1-565/MUC-60) with a secondary electron overview image in the middle. Close ups of sections of Ca-EMP mappings (Ca) secondary electron images (SE) and backscattered electron images (BSE) are shown. Note that the Ca distribution is reflected by the holey structures seen on the BSE images.

BGD
8, 7953–8000, 2011

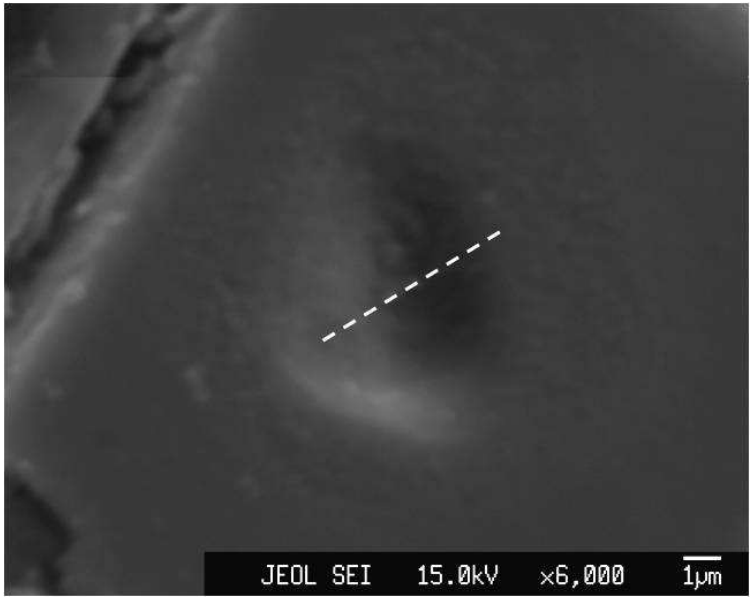

Fig. 9. Secondary electron micrograph of a test section from a *Bolivina spissa* specimen after measuring with SIMS. The spot diameter of the ion beam was about 4–5 µm. Data acquisition time was roughly 10 min. Estimated depth of the spot ~2 µm.

BGD
8, 7953–8000, 2011

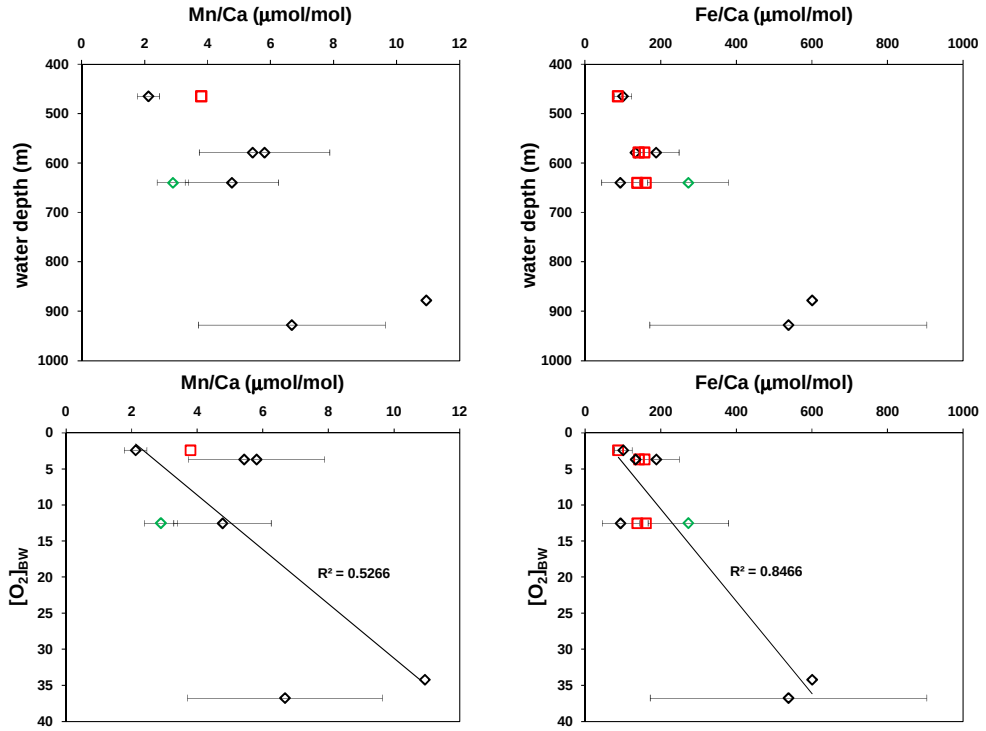

Fig. 10. Mn/Ca and Fe/Ca ratios in tests of *Bolivina spissa* plotted against water depth and $[O_2]_{BW}$. Red squares indicate data points measured on bulk samples of 40 specimens with ICP-MS while diamonds indicate mean values from single specimens measured with SIMS. The specimens indicated by the black diamonds all have been treated with an oxidative cleaning procedure while the single green diamond represents an uncleaned specimen. Error bars on the SIMS data show the standard deviation between the different spots measured on a single specimen. Diamonds without error bars indicate mean values of only two measurements.

BGD
8, 7953–8000, 2011

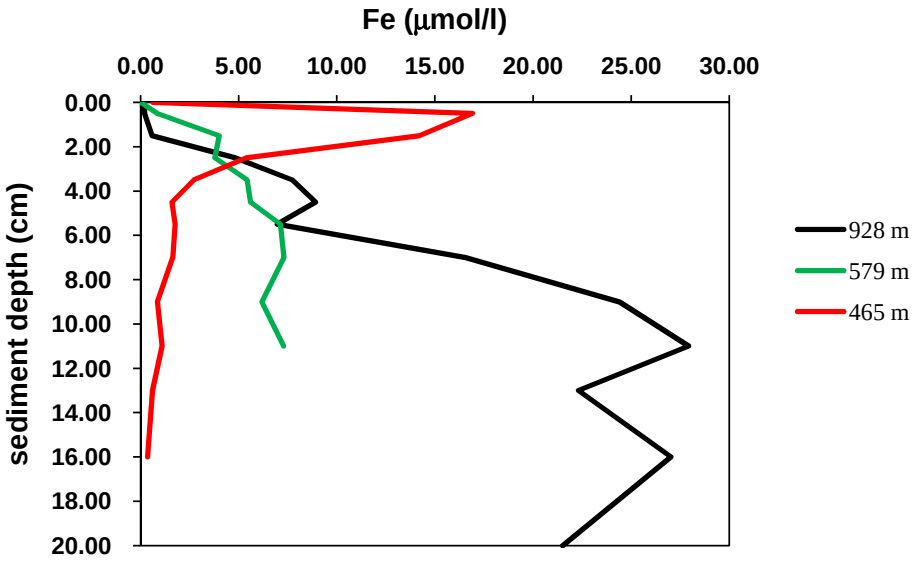

Fig. 11. Fe pore water profiles for different sampling locations at 11° S off Peru (Red: M77-1-455/MUC-21, 465 m. Green: M77-1-487/MUC-38, 579 m. Black: M77-1-445/MUC-15, 928 m).

BGD
8, 7953–8000, 2011

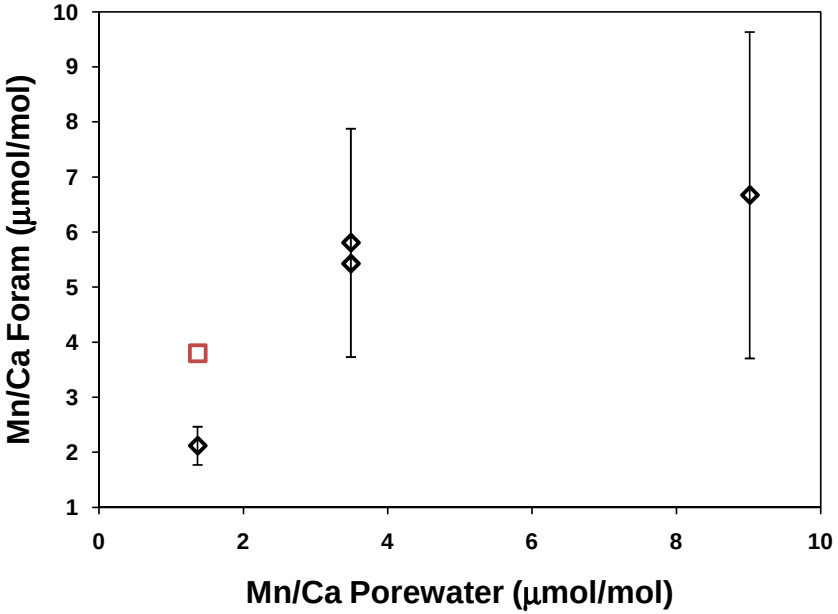

Fig. 12. Correlation between the Mn/Ca ratio in tests of *Bolivina spissa* to the Mn/Ca ratio in the top cm of the pore water from the same sampling location. Red squares indicate data points measured on bulk samples of 40 specimens with ICP-MS while black diamonds indicate mean values from single specimens measured with SIMS. Error bars on the SIMS data show the standard deviation between the different spots measured on a single specimen. Diamonds without error bars indicate mean values of only two measurements.

BGD
8, 7953–8000, 2011

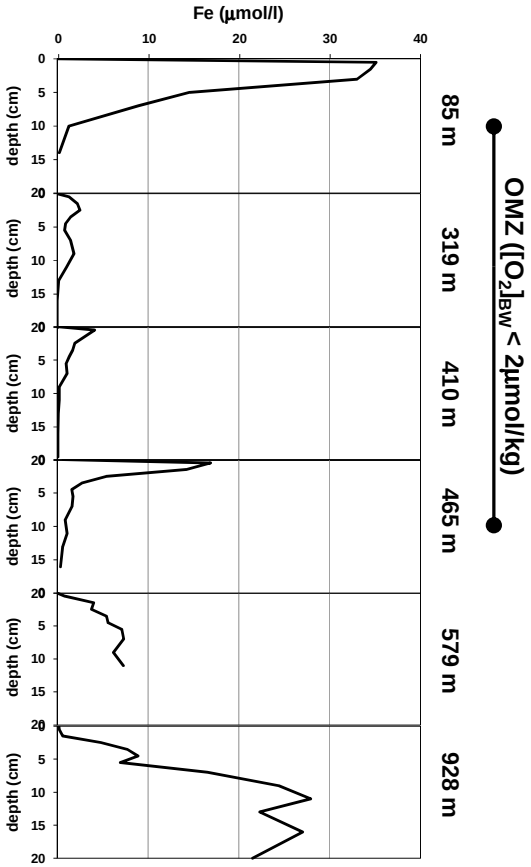

Fig. 13. Pore water profiles for Fe at different water depths at the Peruvian OMZ. The bracket indicates the boundaries of the OMZ where bottom water oxygen concentrations fall below 2 µmol kg^{-1}. Profiles taken from Scholz et al. (2011).

BGD
8, 7953–8000, 2011